ORGANIC CHEMISTRY FRONTIERS

RESEARCH ARTICLE

View Article Online
View Journal | View Issue

Cite this: *Org. Chem. Front.*, 2021, **8**, 5280

Efficient one-pot synthesis of [3]catenanes based on Pt(II) metallacycles with a flexible building block†

Yuan-Guang Shao,[a] Lang He,[a] Qian-Qian Mao,[a] Tao Hong,[a] Xin-Wen Ying,[a] Zibin Zhang,[a] Shijun Li*[a] and Peter J. Stang*[b]

Received 17th June 2021,
Accepted 21st July 2021

DOI: 10.1039/d1qo00910a

rsc.li/frontiers-organic

Two quadrilateral metallacycles were prepared by coordination-driven self-assembly of a 90° platinum(II) receptor **6** with a flexible donor 1,3-bis(4,4′-bipyridinium)propane **1a** or 1,1-bis(4,4′-bipyridinium)methane **1b**, respectively. Three [3]catenanes (**3**, **4** and **5**) were further prepared by *in situ* addition of crown ethers (DB24C8 or DB30C10) to the yielded metallacycles. By comparing the crystal structures of **1a** and **4**, it was found that the bite angle change of the flexible bidentate donor **1a** (111.0° to 112.3°) is much smaller than that of rigid platinum(II) receptor **6** (90.0° to 83.2°) during metalla-cyclization. The multicomponent [3]catenanes were stabilized by multiple supramolecular interactions, including metal coordination, π–π stacking, charge transfer, and hydrogen bonding.

Introduction

Mechanically interlocked molecules (MIMs) are molecules consisting of subcomponents that are connected by mechanical bonds.[1] They have gained much attention from chemists because of not only their unique topological architectures but also their prosperous applications in molecular machines, molecular devices, and smart materials.[2] Catenanes are a type of MIM composed of two or more mechanically interlocked macrocyclic parts.[3] In the past three decades, template-directed strategies for the synthesis of catenanes and other MIMs, such as rotaxanes, Solomon links, and Borromean rings and knots, have been developed impressively.[4] However, the highly efficient preparation of catenanes is still a challenge due to the formation of unexpected polymeric or non-interlocked species during the macrocyclization processes.[3e–g] In particular, when kinetically controlled reactions are used in the final interlocking step, the thermodynamically favorable but kinetically unfavorable nature of macrocyclization processes will hinder the formation of interlocked products. Instead, the use of dynamic covalent chemistry (DCC, such as imine bond formation, disulfide bond formation, and olefin metathesis) and coordination bonds in the final interlocking step can promote the transformations of unexpected intermediates and byproducts into thermodynamically favored MIMs.[5] The reversible feature enables product distribution under thermodynamic control, which means that the MIMs with higher thermodynamic stability will be produced with higher efficiency as the reaction reaches an equilibrium.[6]

Coordination-driven self-assembly has great advantages, including various but predictable geometries, high bonding energy, good bond direction and good reversibility.[7] These intrinsic features make it a promising method for the construction of discrete supramolecular coordination complexes (SCCs). A variety of metallacycles, metallacages and other discrete SCCs with fascinating architectures have been prepared through rational design and careful selection of the metal and organic ligands.[7,8] Because of its modularity and versatility, coordination-driven self-assembly is also a powerful and facile route to provide metal-based macrocyclic supramolecular elements[9] for the construction of MIMs from simple precursors.[10] A number of metal-connected MIMs, including catenanes, rotaxanes, molecular necklaces, Solomon links, and Borromean rings and konts, have been constructed by using this method.[11] The complementary building blocks used in coordination-driven self-assembly are usually structurally rigid conjugated molecules with predefined bite angles.[7] However, the balance of flexibility and rigidity of the ligands also plays a key role in the construction of SCCs. Building blocks with certain flexibility can allow dynamic adaption in the coordination-driven self-assembly, but very flexible linkers are not applicable in most cases. The balance of flexibility and rigidity

[a]*College of Material, Chemistry and Chemical Engineering, Hangzhou Normal University, Hangzhou 311121, China. E-mail: l_shijun@hznu.edu.cn*
[b]*Department of Chemistry, University of Utah, 315 South 1400 East, Room 2020, Salt Lake City, Utah 84112, USA. E-mail: stang@chem.utah.edu*

†Electronic supplementary information (ESI) available: NMR and mass spectra of the guests, metallacycles and catenanes, host–guest complexation investigation and X-ray analysis data of the guest **1a** and catenane **4**. CCDC 2079026 and 2079027. For ESI and crystallographic data in CIF or other electronic format see DOI: 10.1039/d1qo00910a

is also significant in the preparation of catenanes. The use of considerably long and highly flexible linkers usually results in the formation of [2]catenanes during the cyclization processes.[3h] In order to obtain high-order catenanes with more subcomponents, shorter linkers with less flexibility are generally selected. Previously, we have reported the fabrication of metallacycles and metalla-catenanes through Pt(II)-based coordination-driven self-assembly using the 1,2-bis(pyridinium) ethane/dibenzo-24-crown-8 (DB24C8) recognition motif, wherein 1,2-bis(pyridinium)ethane with a slightly flexible ethylene linker acted as a 180° building block.[12] Herein, we want to see whether a more flexible donor with a propylene linker, 1,3-bis(pyridinium)propane, can be used in the construction of SCCs and what bite angle it will have. As monitored by ^{1}H NMR, ^{31}P NMR, and mass spectroscopy and X-ray crystallography analyses, we found that not only quadrilateral metallacycles but also metalla-[3]catenanes can be efficiently prepared by employing this flexible bidentate donor.

From the reported results of Peinador[13] and us,[12] we knew that the bite angles of 1,1-bis(pyridinium)methane and 1,2-bis(pyridinium)ethane were about 109° and 180°, respectively. We speculated that if the sp^3-hybridized propylene carbons are all in stable staggered conformations, the bite angle of 1,3-bis(pyridinium)propane should also be around 109° (Fig. S29†). Therefore, although 1,3-bis(pyridinium)propane is more flexible and has more conformers, it may coordinate with metal acceptors to form metallacycles like 1,1-bis(pyridinium) methane. Herein, both 1,3-bis(4,4′-bipyridinium)propane and 1,1-bis(4,4′-bipyridinium)methane were investigated and compared with each other as the building blocks for the Pt(II)-based coordination-driven self-assembly of metallacycles and metalla-catenanes.

Results and discussion

Synthesis of the bis(4,4′-bipyridinium) guests 1a and 1b

As shown in Scheme 1, 1,3-bis(4,4′-bipyridinium)propane **1a** and 1,1-bis(4,4′-bipyridinium)methane **1b** were conveniently synthesized by *N*-alkylation of 4,4′-bipyridine and then exchange of anions. Their structures were well characterized by nuclear magnetic resonance (NMR) spectroscopy and electrospray ionization mass (ESI-MS) spectrometry (Figs. S1–S4†).

The crystals of **1a** were obtained by vapor diffusion of isopropyl ether into its acetone solution. The single-crystal X-ray analysis (Fig. 1) indicated that the two bipyridinium units of

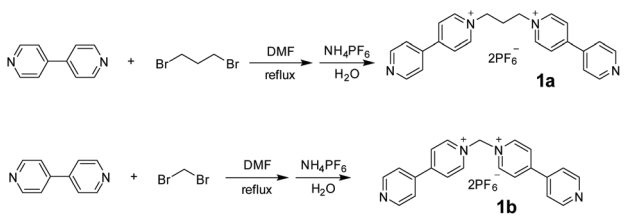

Scheme 1 Synthesis of pyridinium-derived guests **1a** and **1b**.

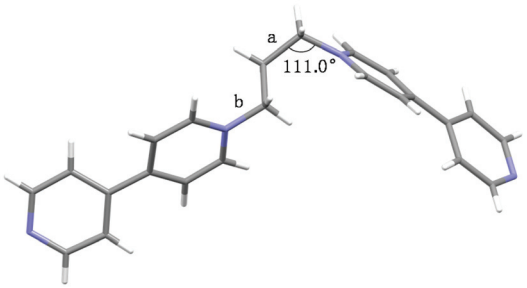

Fig. 1 The crystal structure of **1a**. The counterions have been omitted for clarity. Color code: gray = C; white = H; blue = N.

1a are non-coplanar. Because the three propylene carbons on **1a** are arranged in the staggered conformations and the C–C bond (Fig. 1a) and N–C bond (Fig. 1b) are basically parallel, the bite angle between the two pyridinium groups should be the same as the C–C–N angle (111.0°), which is a little smaller than that of **1b** shown in its crystal structure (112.3°) reported by Peinador and Quintela (Fig. S29†).[13b]

Investigation of the host–guest complexation of DB24C8 ⊃ 1a and DB30C10 ⊃ 1a

Since the host–guest complexation of **1a** with crown ethers has never been reported, we firstly investigated their complexation in acetone. The ^{1}H NMR spectra (Fig. 2) of its mixture solutions with equivalent DB24C8 or DB30C10 (dibenzo-30-crown-10) showed obvious changes on both hosts and **1a**. Peaks of H^a, H^b, H^c, H^d and H^e on the guest **1a**, the aromatic protons H^1 and H^2 on DB24C8, and the protons $H^{1'}$, $H^{2'}$, $H^{3'}$ and $H^{4'}$ on DB30C10 all shifted upfield, while H^3, H^4, H^5, $H^{5'}$ and $H^{6'}$ moved downfield. Only one set of peaks were found in the ^{1}H NMR spectra of the mixed solutions (Fig. 2b and d), indicating that both of the complexation of DB24C8 ⊃ **1a** and DB30C10 ⊃ **1a** are fast-exchange systems on the NMR timescale. The Job plots[14] (Figs. S22 and S24†) based on the ^{1}H NMR spectro-

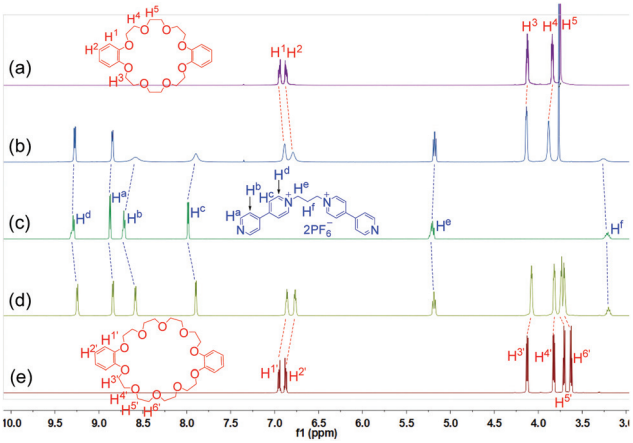

Fig. 2 Partial ^{1}H NMR spectra (500 MHz, acetone-d_6, 25 °C) of 12.00 mM DB24C8 (a), 12.00 mM **1a** + 12.00 mM DB24C8 (b), 12.00 mM **1a** (c), 12.00 mM **1a** + 12.00 mM DB30C10 (d), and 12.00 mM DB30C10 (e).

scopic data demonstrated that complexes of **1a** with both DB24C8 and DB30C10 have 1 : 1 stoichiometry in solutions.

Furthermore, the 1 : 1 stoichiometry was confirmed by their ESI-MS spectra. One main peak was observed for [DB24C8 ⊃ **1a** − PF_6]$^+$: *m*/*z* = 947.3587, and one minor peak was found for [[DB24C8]$_2$ ⊃ **1a** − PF_6]$^+$: *m*/*z* = 1395.5655 (Fig. S23†). Nonetheless, the latter is found in very small abundance, indicating that they mainly formed a 1 : 1 complex in solution. Two relevant peaks were found for the complex of DB30C10 ⊃ **1a** with 1 : 1 stoichiometry, [DB30C10 ⊃ **1a** − PF_6]$^+$: *m*/*z* = 1035.42387 and [DB30C10 ⊃ **1a** − 2PF_6]$^{2+}$: *m*/*z* = 445.2301 (Fig. S25†). No peaks were observed for the complexes with other stoichiometries. The association constant (K_a) values of DB24C8 ⊃ **1a** and DB30C10 ⊃ **1a** were determined to be 2620 (±200) M^{-1} and 1490 (± 120) M^{-1}, respectively, in CH_3CN by using the UV-vis titration method (Figs. S27 and S28†). Both of them are higher than the previously reported association constant[13b] of DB24C8 ⊃ **1b**, 915 ± 35 M^{-1}, in CH_3CN, probably because the longer propylene linker with higher flexibility is more space-matching and enables better dynamic adaption to be complexed by the crown ethers than the shorter methylene linker.

Preparation of the quadrilateral metallacycles 2a and 2b

As the flexible bis(4,4′-bipyridinium)propane **1a** has a similar coordination angle to **1b**, it was supposed that it could coordinate with a 90° platinum(II) acceptor to form discrete quadrilateral metallacycles such as **1b**.[13] An acetone-d_6 solution of **1a** or **1b** was stirred with an equimolar 90° Pt(II) receptor (**6**) at room temperature, which gave rise to the formation of metal assemblies **2a** and **2b**, respectively (Scheme 2). The ^{1}H and ^{31}P{^{1}H} NMR spectra of **2a** and **2b**, together with their ^{1}H–^{1}H COSY (correlation spectroscopy) NMR spectra and mass spectrometry, provided solid evidence for the formation of discrete metallacycles. Both the ^{31}P{^{1}H} NMR spectra of **2a** and **2b** displayed a singlet at −0.30 ppm and −0.23 ppm, respectively, accompanied by a set of symmetrical and uniformed ^{195}Pt satellites, which was consistent with the Pt–N coordination environment (Fig. S6 and S9†). All peaks in their ^{1}H NMR (Fig. S5 and S8†) and ^{1}H–^{1}H COSY NMR spectra (Fig. S7 and S10†) were also clearly assigned. Although the X-ray crystal structure shows a nearly 109° bite angle of **1a** in the solid state (Fig. 1), other conformations with slightly different bite angles may exist in solution where the assembly was performed due to its relatively higher flexibility. In the ^{1}H NMR spectrum of **2a**, we observed tiny impure peaks that might belong to the isomeric self-assembly species resulting from the conformational isomerism of the propylene linker. In comparison, no visible impure peaks were found in the ^{1}H NMR spectrum of **2b**, which could be due to the less flexibility of ligand **1b**. The ESI-MS measurements further supported the formation of metallacycles **2a** and **2b**. The ESI-MS spectrum of metallacycle **2a** (Fig. S17†) showed two related peaks at *m*/*z* = 1224.2068 and 1228.1958, attributed to [M − 2OTf]$^{2+}$ and [M − 2PF_6]$^{2+}$, respectively. For the metallacycle **2b** (Fig. S18†), one peak at *m*/*z* = 1383.2289 was observed corresponding to [M + 2K]$^{2+}$.

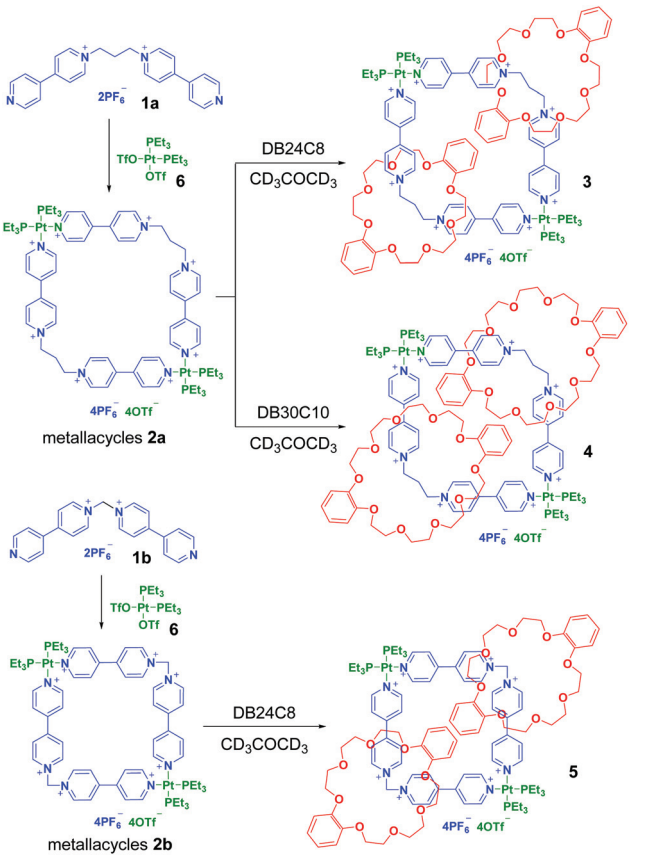

Scheme 2 Synthesis of metallacycles **2a** and **2b** and [3]catenanes **3**, **4**, and **5**.

Synthesis of [3]catenanes 3, 4 and 5

Because of the dynamic nature of the coordination interactions, the *in situ* addition of crown ethers into the prepared metallacycles **2** resulted in the generation of catenanes. [3]Catenanes **3** and **5** were fabricated by the addition of DB24C8 into the solutions of **2a** or **2b** (3.0 mM), respectively, at room temperature, while [3]catenane **4** was obtained by the addition of DB30C10 (18.0 mM) into a solution of **2a** (3.0 mM). Directly mixing the precursors (**1** + **6** + crown ether) in one pot also led to the same results (Fig. S30–35†). After the addition of crown ethers, all the solutions changed from colorless to yellow, which indicated that charge-transfer interactions existed between crown ethers and electron-poor guests.

The dynamic threading processes of metallacycles **2** (**2a** or **2b**) and crown ether (DB24C8 or DB30C10) were observed real-time by ^{31}P{^{1}H} and ^{1}H NMR spectroscopy. When DB24C8 was added into a 3.0 mM solution of **2a**, a new set of peaks corresponding to [3]catenane **3** appeared in the ^{31}P{^{1}H} NMR spectra (Fig. 3). As the amount of DB24C8 increased, **2a** gradually converted into **3**. Finally, when 18.0 mM DB24C8 was added, the peak related to free metallacycle **2a** almost completely disappeared (Fig. 3d). The same trend was also observed in the ^{1}H NMR spectra (Fig. 4). When 6.0 mM DB24C8 was added into a 3.0 mM solution of **2a**, the characteristic peaks indicated

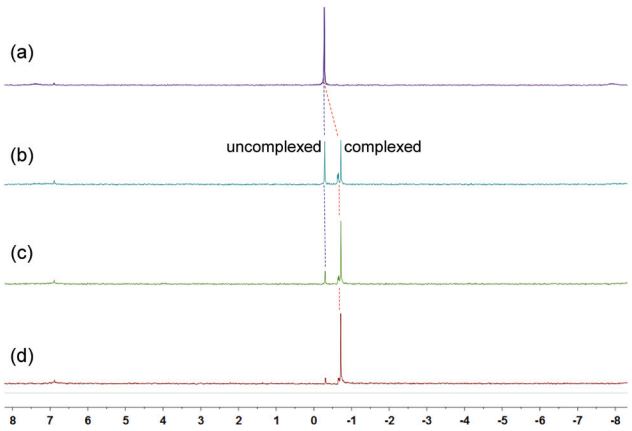

Fig. 3 $^{31}P\{^{1}H\}$ NMR (202 MHz, acetone-d_6, 25 °C) spectra of metallacycle **2a** (3.0 mM) (a), **2a** (3.0 mM) + DB24C8 (6.0 mM) (b), **2a** (3.0 mM) + DB24C8 (12.0 mM) (c), and **2a** (3.0 mM) + DB24C8 (18.0 mM) (d).

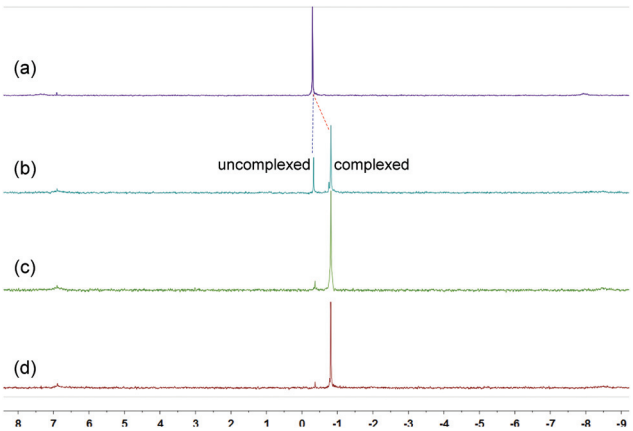

Fig. 5 $^{31}P\{^{1}H\}$ NMR (202 MHz, acetone-d_6, 25 °C) spectra of metallacycle **2a** (3.0 mM) (a), **2a** (3.0 mM) + DB30C10 (6.0 mM) (b), **2a** (3.0 mM) + DB30C10 (12.0 mM) (c), and **2a** (3.0 mM) + DB30C10 (18.0 mM) (d).

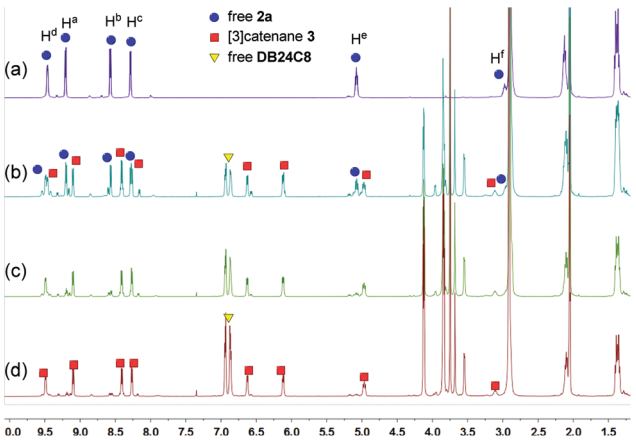

Fig. 4 ^{1}H NMR (500 MHz, acetone-d_6, 25 °C) spectra of metallacycle **2a** (3.0 mM) (a), **2a** (3.0 mM) + DB24C8 (6.0 mM) (b), **2a** (3.0 mM) + DB24C8 (12.0 mM) (c), and **2a** (3.0 mM) + DB24C8 (18.0 mM) (d).

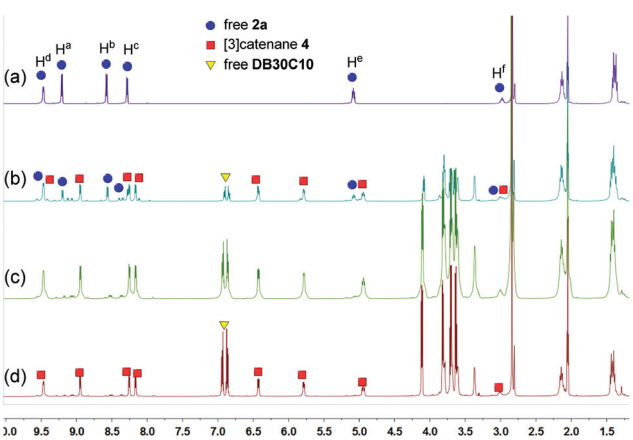

Fig. 6 ^{1}H NMR (500 MHz, acetone-d_6, 25 °C) spectra of metallacycle **2a** (3.0 mM) (a), **2a** (3.0 mM) + DB30C10 (6.0 mM) (b), **2a** (3.0 mM) + DB30C10 (12.0 mM) (c), and **2a** (3.0 mM) + DB30C10 (18.0 mM) (d).

that the solution mainly contained three different species, the free DB24C8, the free metallacycle **2a** and the threaded [3]catenane **3**. After more DB24C8 was added, the peaks of **2a** decreased gradually. Finally, [3]catenane **3** was formed as the main product (Fig. 4d). Like the host–guest complexation of DB24C8 ⊃ **1a**, all aromatic hydrogen signals of the guest moiety **2a** shifted upfield, mostly because of the shielding effect and the increase of electron density originated from the charge transfer and CH–O hydrogen bonds, after the formation of **3**. The slight upfield shift of the phosphorus signal of **2a** should also be attributed to the enrichment of the electron density of **2a** after its complexation with the electron-rich crown ethers.

These changes in the $^{31}P\{^{1}H\}$ and ^{1}H NMR spectra all indicated the gradual formation of [3]catenane **3**. Similar changes were also observed for **4** (Fig. 5 and 6) and **5** (Fig. 7 and 8). Since there was no great difference in the association constants of DB24C8 ⊃ **1a**, DB30C10 ⊃ **1a** and DB24C8 ⊃ **1b**,

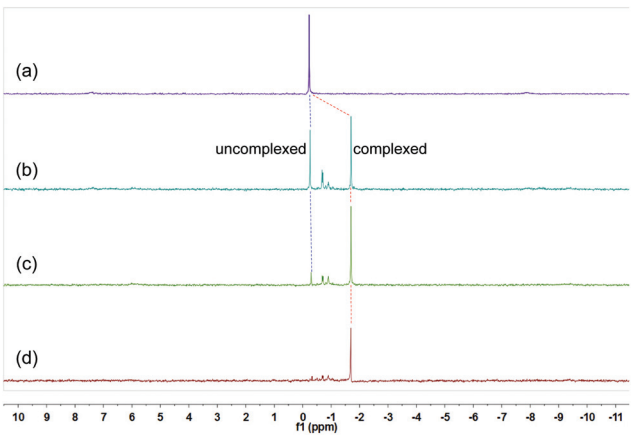

Fig. 7 $^{31}P\{^{1}H\}$ NMR (202 MHz, acetone-d_6, 25 °C) spectra of metallacycle **2b** (3.0 mM) (a), **2b** (3.0 mM) + DB24C8 (6.0 mM) (b), **2b** (3.0 mM) + DB24C8 (12.0 mM) (c), **2b** (3.0 mM) + DB24C8 (18.0 mM) (d).

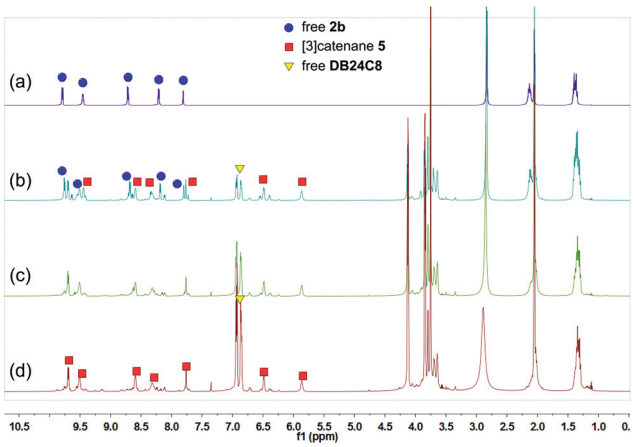

Fig. 8 ^{1}H NMR (500 MHz, acetone-d_6, 25 °C) spectra of metallacycle **2b** (3.0 mM) (a), **2b** (3.0 mM) + DB24C8 (6.0 mM) (b), **2b** (3.0 mM) + DB24C8 (12.0 mM) (c), and **2b** (3.0 mM) + DB24C8 (18.0 mM) (d).

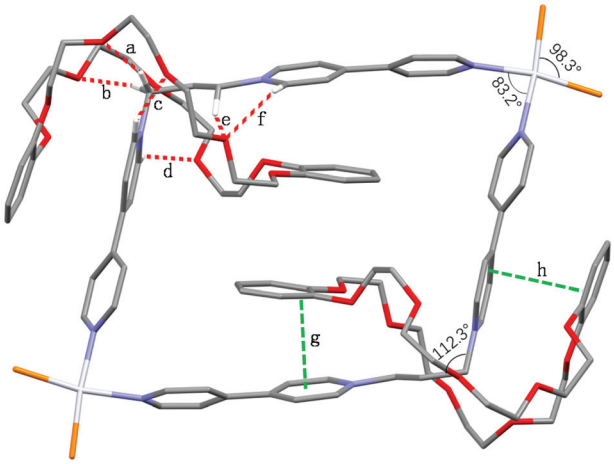

Fig. 9 Single-crystal X-ray structure of [3]catenane **4**. The ethyl groups on phosphines, counterions, and H atoms, except for the ones involved in hydrogen bonding, have been omitted for clarity. Hydrogen bond parameters: H···O distance (Å), C–H···O angle (deg); a, 2.314, 161.3; b, 2.396, 159.6; c, 2.400, 158.5; d, 2.403, 137.5; e, 2.549, 133.2; f, 2.541, 141.5. Color code: gray = C; red = O; white = H; blue = N; white = Pt; orange = P.

the amounts of crown ethers for complete conversion from free metallacycles to the [3]catenanes **3**, **4** and **5** were almost the same.

ESI-MS studies further supported the formation of [3]catenanes. A few peaks belonging to the intact catenanes were found in their MS spectra, but some of them overlapped with their half-fragment peaks (Fig. S19–S21†). Therefore, we further exchanged the mixed counteranions of OTf^- and PF_6^- to be unified PF_6^-. The detailed exchange procedures are provided in the ESI.† ^{1}H and $^{31}P\{^{1}H\}$ NMR spectra of the anion-exchanged metallacycles (**7** and **8**) and catenanes (**9**, **10** and **11**) (Fig. S36–S45†) indicated that the exchange of anions did not affect their structures. In the MS spectra of the anion-exchanged [3]catenanes, the overlapped half-fragment peaks did not appear. Four related peaks were observed in the MS spectrum of anion-exchanged [3]catenane **9** at m/z = 1668.8662, 1064.3447, 1893.1202 and 1533.5529, attributed to $[M - 2PF_6]^{2+}$, $[M - 3PF_6]^{3+}$, $[M + 2MeOH + H_2O + 2K]^{2+}$ and $[M - 4HPF_6 + H + Na]^{2+}$, respectively (Fig. S46†). For [3]catenane **10**, three peaks relevant to the intact [3]catenane self-assembly were found at m/z = 1757.0630, 1122.7149 and 1339.5517, corresponding to $[M - 2PF_6]^{2+}$, $[M - 3PF_6]^{3+}$ and $[M - 8HPF_6 + Na + NH_4]^{2+}$, respectively (Fig. S47†). The ESI-MS spectrum of [3]catenane **11** (Fig. S48†) showed one peak at m/z = 1785.5858, corresponding to $[M + 2H]^{2+}$.

Moreover, the formation of [3]catenanes was unambiguously confirmed by single-crystal X-ray analysis (Fig. 9). The X-ray-quality yellow crystals of [3]catenane **4** were obtained by slow diffusion of methanol into an acetone solution of **2a** (3.0 mM) with excess DB30C10 (18.0 mM). The crystal structure of **4** revealed that the bite angle between the two pyridinium groups (112.3°) almost remains the same as that in the free ligand **2a** (111.0°, Fig. 1) and the coordination angle of N–Pt–N reduced 6.8° (from the ideal Pt(II) square coordination angle of 90.0° to 83.2°) to meet the demands for the quadrilateral metallacycle with the guest **1a**. Two DB30C10 molecules thread into the metallacycle **2a** with an S-shaped conformation and symmetrically locate on the two diagonal corners of the metallacycle, that is, complex around the propylene groups. The two phenyl rings on the crown ethers are almost parallel to the bipyridine units on the guests inside and outside the metallacycle, and the distances are about 3.5 Å (g and h in Fig. 9), which is a favorable distance for π–π stacking interactions. At the same time, the phenyl rings on the two crown ethers inside the metallacycle are also parallel to each other. Additionally, the ether oxygen atoms of DB30C10 have strong hydrogen bond interactions (a–f in Fig. 9) with some of the hydrogen atoms on the propylene groups or on the pyridinium rings of **1a**, which not only stabilize the conformations of the host–guest complex but also strengthen the rigidity of the propylene linker.

Conclusions

In summary, we synthesized a flexible bidentate ligand bis(4,4′-bipyridinium)propane **1a** using bis(4,4′-bipyridinium) methane **1b** as a control compound, which could complex with DB24C8 or DB30C10 with high association constants. By coordination-driven self-assembly of these two donors and a 90° platinum(II) receptor, two quadrilateral metallacycles were fabricated efficiently. Taking advantage of the dynamic coordination bonds, three [3]catenanes were obtained quantitatively by the *in situ* threading of **2** into the crown ethers. By comparing the crystal structures of the free ligand **1a** and the coordinated one in [3]catenane **4**, it was found that the bite angle between the two pyridinium groups almost remains the same after the formation of the [3]catenane. The bite angle between the two pyridinium groups either in the free ligand **2a**

or in the [3]catenane is slightly higher than 109°, while the bite angle of N–Pt–N decreased to 83.2° from the ideal Pt(II) square coordination angle of 90.0° to meet the demands for the formation of the quadrilateral metallacycle. It was believed that the wrapping of crown ethers turns the flexible propylene-linked bidentate ligands **1a** rigid and the large bite angle of **1a** makes the platinum(II) receptor **6** an adaptable building block in the [3]catenanes. In the future, we will focus on the investigation of ligands with controllable bite angles and their applications in transformable SCCs or molecular machines.

Experimental section

Materials and methods

Unless otherwise noted, materials were obtained from commercial suppliers and used without further purification. Solvents were either employed as purchased or dried according to procedures described in the literature. Column chromatography was performed over silica gel (200–300 mesh). NMR spectra were collected on a Bruker AVANCE DMX-500 spectrometer at room temperature. All NMR data are reported in ppm. $^{31}P\{^1H\}$ NMR chemical shifts are referenced to an external unlocked sample of 85% H_3PO_4 (δ 0.0), while ^1H NMR and $^{13}C\{^1H\}$ NMR chemical shifts are reported relative to the residual peak of the deuterated solvents or internal standard tetramethylsilane (TMS). ESI-MS spectra were obtained on an Agilent 1290-6530 UPLC-Q-TOF spectrometer using electrospray ionization. Crystal data were collected on a Bruker D8 Venture (Billerica, Massachusetts, USA). The melting points were measured using a Melting Point M-565 apparatus.

Synthesis of 1,3-bis(4,4′-bipyridinium)propane 1a. A solution of 4,4′-bipyridine (11.60 g, 74.30 mmol) and 1,3-dibromopropane (1.50 g, 7.43 mmol) in DMF (80 mL) was refluxed for 2 days. After cooling to room temperature, the yellow precipitate was filtered and washed with a small amount of DMF to afford a solid which was then re-dissolved in water (15 mL). An excess of NH_4PF_6 was added to the solution until no further precipitation was observed. The resulted residue was purified by flash column chromatography (methanol/2 M NH_4Cl aqueous solution/nitromethane = 20 : 2 : 1) and then anion-exchanged by using NH_4PF_6 and dried to afford **1a** as a white solid (1.10 g, 23%). M.P. 270–272 °C. ^1H NMR (500 MHz, CD_3CN) δ (ppm) 8.86 (dd, J = 4.5, 1.7 Hz, 4H), 8.80 (d, J = 6.9 Hz, 4H), 8.38 (d, J = 6.9 Hz, 4H), 7.80 (dd, J = 4.5, 1.7 Hz, 4H), 4.72–4.68 (m, 4H), 2.74–2.68 (m, 2H). ^{13}C NMR (126 MHz, CD_3CN) δ (ppm) 155.8, 152.3, 146.1, 142.0, 127.4, 122.8, 58.7, 32.7. ESI-TOF-MS (m/z): calcd for $C_{23}H_{22}F_6N_4P$ $[M - PF_6]^+$: 499.1481, found: 499.1468.

Synthesis of 1,1-bis(4,4′-bipyridinium)methane 1b.[13b] A solution of 4,4′-bipyridine (3.37 g, 21.57 mmol) and dibromomethane (1.50 g, 8.63 mmol) in DMF (50 mL) was refluxed for 2 days. After cooling to room temperature, the yellow precipitate was filtered and washed with a small amount of DMF to afford a solid which was then re-dissolved in water (15 mL). An excess of NH_4PF_6 was added to the solution until no further precipitation was observed. The solid was filtered and washed with cold water to afford **1b** as a white solid (2.40 g, 45%). ^1H NMR (500 MHz, acetone-d_6) δ (ppm) 9.84 (d, J = 7.0 Hz, 4H), 8.90–8.88 (m, 8H), 8.00 (dd, J = 4.5, 1.6 Hz, 4H), 7.90 (s, 2H).

Synthesis of metallacycle 2a. The 90° Pt(II) precursor (**6**) (4.38 mg, 0.006 mmol) and **1a** (3.87 mg, 0.006 mmol) were placed in a 2-dram vial, followed by the addition of acetone-d_6 (0.6 mL). After 5 h of stirring at room temperature, the reaction solution was directly used for characterization. ^1H NMR (500 MHz, acetone-d_6,) (Fig. S5†): δ (ppm) 9.47 (d, J = 4.8 Hz, 8H), 9.21 (d, J = 7.0 Hz, 8H), 8.58 (d, J = 7.0 Hz, 8H), 8.29 (d, J = 6.6 Hz, 8H), 5.13–5.04 (m, 8H), 3.02–2.95 (m, 4H), 2.18–2.09 (m, 24H), 1.38 (dt, J = 17.5, 7.5 Hz, 36H). $^{31}P\{^1H\}$ NMR (202 MHz, acetone-d_6) (Fig. S6†): δ (ppm) −0.30 (s, ^{195}Pt satellites, J_{Pt-P} = 3087 Hz). ESI-TOF-MS (m/z): calcd for calcd for $[M - 2PF_6]^{2+}$: 1228.1934, found: 1228.1958; $[M - 2OTf]^{2+}$: 1224.2094, found: 1224.2068.

Synthesis of metallacycle 2b. The 90° Pt(II) precursor (**6**) (4.38 mg, 0.006 mmol) and **1b** (3.69 mg, 0.006 mmol) were placed in a 2-dram vial, followed by the addition of acetone-d_6 (0.6 mL). After 5 h of stirring at room temperature, the reaction solution was directly used for characterization. ^1H NMR (500 MHz, acetone-d_6) (Fig. S8†): δ (ppm) 9.79 (d, J = 6.9 Hz, 8H), 9.45 (d, J = 4.9 Hz, 8H), 8.72 (d, J = 6.9 Hz, 8H), 8.21 (d, J = 6.4 Hz, 8H), 7.81 (s, 4H), 2.20–2.09 (m, 24H), 1.38 (dt, J = 17.3, 7.4 Hz, 36H). $^{31}P\{^1H\}$ NMR (202 MHz, acetone-d_6) (Fig. S9†): δ (ppm) −0.23 (s, ^{195}Pt satellites, J_{Pt-P} = 3089 Hz). ESI-TOF-MS (m/z): calcd for $[M + 2K]^{2+}$: 1383.1305, found: 1383.2289.

Synthesis of [3]catenane 3. Various equivalents of DB24C8 (see Fig. 3 and 4) were added directly into a solution of metallacycle **2a** in acetone-d_6. The mixture was then stirred for 2 days at room temperature to generate [3]catenane **3**. This initial reaction solution was directly used for the following characterization. ^1H NMR (500 MHz, acetone-d_6) (Fig. S11†): δ (ppm) 9.49 (d, J = 5.1 Hz, 8H), 9.10 (d, J = 6.7 Hz, 8H), 8.41 (d, J = 6.7 Hz, 8H), 8.26 (d, J = 6.3 Hz, 8H), 6.63 (dd, J = 5.8, 3.7 Hz, 8H), 6.12 (dd, J = 5.9, 3.4 Hz, 8H), 4.99–4.93 (m, 8H), 3.83 (s, 16H), 3.68 (s, 16H), 3.54 (d, J = 5.6 Hz, 16H), 3.10 (br, 4H), 2.15–2.08 (m, 24H), 1.40–1.34 (m, 36H). $^{31}P\{^1H\}$ NMR (202 MHz, acetone-d_6) (Fig. S12†): δ (ppm) −0.71 (s, ^{195}Pt satellites, J_{Pt-P} = 3101 Hz). ESI-TOF-MS (m/z): calcd for $[M - 2PF_6]^{2+}$: 1676.4032, found: 1676.4027; calcd for $[M - 2OTf]^{2+}$: 1672.4153, found: 1672.4119.

Synthesis of [3]catenane 4. Various equivalents of DB30C10 (see Fig. 5 and 6) were added directly into a solution of metallacycle **2a** in acetone-d_6. The solution was then stirred for 2 days at room temperature to generate [3]catenane **4**. This initial reaction solution was directly used for the following characterization. ^1H NMR (500 MHz, acetone-d_6) (Fig. S13†): δ (ppm) 9.47 (d, J = 4.8 Hz, 8H), 8.95 (d, J = 6.8 Hz, 8H), 8.25 (d, J = 6.8 Hz, 8H), 8.17 (d, J = 6.6 Hz, 8H), 6.48–6.40 (m, 8H), 5.84–5.75 (m, 8H), 4.99–4.90 (m, 8H), 3.81–3.78 (m, 16H), 3.68 (dd, J = 5.2, 3.3 Hz, 16H), 3.61 (d, J = 4.6 Hz, 16H), 3.37 (d, J = 2.7 Hz, 16H), 3.04–2.98 (m, 4H), 2.18–2.10 (m, 24H), 1.42 (dt, J = 17.4, 7.5 Hz, 36H). $^{31}P\{^1H\}$ NMR (202 MHz, acetone-d_6) (Fig. S14†): δ (ppm) −0.81 (s, ^{195}Pt satellites, J_{Pt-P} = 3111 Hz). ESI-TOF-MS (m/z): calcd for $[M - 2OTf]^{2+}$: 1760.4678, found:

1760.4725; calcd for $[M - 2PF_6]^{2+}$: 1764.4556, found: 1764.4629; calcd for $[M - 3OTf]^{3+}$: 1123.9968, found: 1123.9954.

Synthesis of [3]catenane 5. Various equivalents of DB24C8 (see Fig. 7 and 8) were added directly into a solution of metallacycle **2b** in acetone-d_6. The solution was then stirred for 2 days at room temperature to generate [3]catenane **5**. This initial reaction solution was directly used for the following characterization. ^{1}H NMR (500 MHz, acetone-d_6) (Fig. S15†): δ (ppm) 9.69 (d, J = 6.9 Hz, 8H), 9.51 (s, 8H), 8.59 (d, J = 6.4 Hz, 8H), 8.32 (s, 8H), 7.76 (s, 4H), 6.50–6.46 (m, 8H), 5.86 (s, 8H), 3.80 (s, 16H), 3.69 (d, J = 5.0 Hz, 16H), 3.65 (s, 16H), 2.02–2.00 (m, 24H), 1.35–1.30 (m, 36H). ^{31}P{^{1}H} NMR (202 MHz, acetone-d_6) (Fig. S16†): δ (ppm) −1.64 (s, ^{195}Pt satellites, J_{Pt-P} = 3141 Hz). ESI-TOF-MS (m/z): calcd for $[M - 2PF_6]^{2+}$: 1648.3718, found: 1648.3750; calcd for $[M - 2OTf]^{2+}$: 1644.3879, found: 1644.3840.

Author contributions

Investigation, Y. S., L. H., Q. M., T. H., and X. Y.; writing – original draft, Y. S. and Z. Z.; funding acquisition and project administration, S. L.; conceptualization, supervision, validation, and writing – review and editing, S. L. and P. S. All authors have read and agreed to the published version of the manuscript.

Conflicts of interest

There are no conflicts to declare.

Acknowledgements

This work was supported by the National Natural Science Foundation of China (21572042 and 21773052), the Program for Changjiang Scholars and Innovative Research Team in the Chinese University (IRT 1231), and the Science & Technology Innovation Program of Zhejiang Province (2018R52051). The authors thank Jiyong Liu (Department of Chemistry, Zhejiang University, Hangzhou 310027, P. R. China) for the single-crystal characterization of **1a** and **4**.

References

1 (*a*) *Molecular catenanes, rotaxanes and knots*, ed. J.-P. Sauvage and C. Dietrich-Buchecker, Wiley-VCH, Weinheim, 1999; (*b*) R. S. Forgan, J.-P. Sauvage and J. F. Stoddart, Chemical topology: complex molecular knots, links, and entanglements, *Chem. Rev.*, 2011, **111**, 5434–5464; (*c*) J. E. Beves, B. A. Blight, C. J. Campbell, D. A. Leigh and R. T. McBurney, Strategies and tactics for the metal-directed synthesis of rotaxanes, knots, catenanes, and higher order links, *Angew. Chem., Int. Ed.*, 2011, **50**, 9260–9327; (*d*) M. Xue, Y. Yang, X. Chi, X. Yan and F. Huang, Development of pseudorotaxanes and rotaxanes: from synthesis to stimuli-responsive motions to applications, *Chem. Rev.*, 2015, **115**, 7398–7501; (*e*) C. J. Bruns and J. F. Stoddart, *The Nature of the Mechanical Bond: From Molecules to Machines*, Wiley, New Jersey, 2017; (*f*) K. M. Bak, K. Porfyrakis, J. J. Davis and P. D. Beer, Exploiting the mechanical bond for molecular recognition and sensing of charged species, *Mater. Chem. Front.*, 2020, **4**, 1052–1073.

2 (*a*) E. R. Kay, D. A. Leigh and F. Zerbetto, Synthetic molecular motors and mechanical machines, *Angew. Chem., Int. Ed.*, 2007, **46**, 72–191; (*b*) Z. Niu and H. W. Gibson, Polycatenanes, *Chem. Rev.*, 2009, **109**, 6024–6046; (*c*) A. Harada, A. Hashidzume, H. Yamaguchi and Y. Takashima, Polymeric rotaxanes, *Chem. Rev.*, 2009, **109**, 5974–6023; (*d*) L. Fang, M. A. Olson, D. Benítez, E. Tkatchouk, W. A. Goddard III and J. F. Stoddart, Mechanically bonded macromolecules, *Chem. Soc. Rev.*, 2010, **39**, 17–29; (*e*) M. Zhang, K. Zhu and F. Huang, Improved complexation of paraquat derivatives by the formation of crown ether-based cryptands, *Chem. Commun.*, 2010, **46**, 8131–8141; (*f*) A. Coskun, M. Banaszak, R. D. Astumian, J. F. Stoddart and B. A. Grzybowski, Great expectations: can artificial molecular machines deliver on their promise?, *Chem. Soc. Rev.*, 2012, **41**, 19–30; (*g*) M. Zhang, X. Yan, F. Huang, Z. Niu and H. W. Gibson, Stimuli-responsive host-guest systems based on the recognition of cryptands by organic guests, *Acc. Chem. Res.*, 2014, **47**, 1995–2005; (*h*) Z. Zhang, K. Sun, L. Jin, C. Xie and S. Li, Preparation of a mechanically interlocked polymer from a linear supramolecular polymer, *Org. Chem. Front.*, 2020, **7**, 1453–1462.

3 (*a*) D. A. Leigh, J. K. Y. Wong, F. Dehez and F. Zerbetto, Unidirectional rotation in a mechanically interlocked molecular rotor, *Nature*, 2003, **424**, 174–179; (*b*) J.-P. Sauvage, Transition metal-complexed catenanes and rotaxanes as molecular machine prototypes, *Chem. Commun.*, 2005, 1507–1510; (*c*) O. Š. Miljanić and J. F. Stoddart, Dynamic donor–acceptor [2]catenanes, *Proc. Natl. Acad. Sci. U. S. A.*, 2007, **104**, 12966–12970; (*d*) M. Liu, S. Li, M. Hu, F. Wang and F. Huang, Selectivity algorithm for the formation of two cryptand/paraquat catenanes, *Org. Lett.*, 2010, **12**, 760–763; (*e*) G. Gil-Ramírez, D. A. Leigh and A. J. Stephens, Catenanes: fifty years of molecular links, *Angew. Chem., Int. Ed.*, 2015, **54**, 6110–6150; (*f*) H. Y. Au-Yeung, C.-C. Yee, A. W. H. Ng and K. Hu, Strategies to assemble catenanes with multiple interlocked macrocycles, *Inorg. Chem.*, 2018, **57**, 3475–3485; (*g*) N. H. Pérez and J. E. M. Lewis, Synthetic strategies towards mechanically interlocked oligomers and polymers, *Org. Biomol. Chem.*, 2020, **18**, 6757–6780; (*h*) F.-Z. Yan, Y.-G. Shao, Z. Zhang, Y.-F. Shen, X.-C. Huang, P.-L. Zhang and S. Li, Synthesis of catenanes from a BMP32C10-based cryptand tuned by the linkage length of paraquat salts, *Synthesis*, 2021, **53**, 338–343; (*i*) R. C. Knighton and P. D. Beer, Sodium cation-templated

synthesis of an ion-pair binding heteroditopic [2]catenane, *Org. Chem. Front.*, 2021, **8**, 2468–2472.

4 (*a*) M. S. Vickers and P. D. Beer, Anion templated assembly of mechanically interlocked structures, *Chem. Soc. Rev.*, 2007, **36**, 211–225; (*b*) J. D. Crowley, S. M. Goldup, A.-L. Lee, D. A. Leigh and R. T. McBurney, Active metal template synthesis of rotaxanes, catenanes and molecular shuttles, *Chem. Soc. Rev.*, 2009, **38**, 1530–1541; (*c*) S. Li, K. Zhu, B. Zheng, X. Wen, N. Li and F. Huang, A bis(*m*-phenylene)-32-crown-10/paraquat [2]rotaxane, *Eur. J. Org. Chem.*, 2009, 1053–1057; (*d*) J. E. M. Lewis, P. D. Beer, S. J. Loeb and S. M. Goldup, Metal ions in the synthesis of interlocked molecules and materials, *Chem. Soc. Rev.*, 2017, **46**, 2577–2591.

5 (*a*) J. M. Lehn, Dynamic combinatorial chemistry and virtual combinatorial libraries, *Chem. – Eur. J.*, 1999, **5**, 2455–2463; (*b*) S. J. Rowan, S. J. Cantrill, G. R. L. Cousins, J. K. M. Sanders and J. F. Stoddart, Dynamic covalent chemistry, *Angew. Chem., Int. Ed.*, 2002, **41**, 898–952; (*c*) P. T. Corbett, J. Leclaire, L. Vial, K. R. West, J. L. Wietor, J. K. M. Sanders and S. Otto, Dynamic combinatorial chemistry, *Chem. Rev.*, 2006, **106**, 3652–3711; (*d*) J. M. Lehn, From supramolecular chemistry towards constitutional dynamic chemistry and adaptive chemistry, *Chem. Soc. Rev.*, 2007, **36**, 151–160; (*e*) F. B. L. Cougnons and J. K. M. Sanders, Evolution of dynamic combinatorial chemistry, *Acc. Chem. Res.*, 2012, **45**, 2211–2221.

6 (*a*) S. Li, M. Liu, B. Zheng, K. Zhu, F. Wang, N. Li, X.-L. Zhao and F. Huang, Taco complex templated syntheses of a cryptand/paraquat [2]rotaxane and a [2]catenane by olefin metathesis, *Org. Lett.*, 2009, **11**, 3350–3353; (*b*) Y. W. Wu, S. T. Tung, C. C. Lai, Y. H. Liu, S. M. Peng and S. H. Chiu, Cyclic [2]catenane dimers, trimers, and tetramers, *Angew. Chem., Int. Ed.*, 2015, **54**, 11745–11749; (*c*) H. Li, H. C. Zhang, A. D. Lammer, M. Wang, X. P. Li, V. M. Lynch and J. L. Sessler, Quantitative self-assembly of a purely organic three-dimensional catenane in water, *Nat. Chem.*, 2015, **7**, 1003–1008; (*d*) S. P. Black, D. M. Wood, F. B. Schwarz, T. K. Ronson, J. J. Holstein, A. R. Stefankiewicz, C. A. Schalley, J. K. M. Sanders and J. R. Nitschke, Catenation and encapsulation induce distinct reconstitutions within a dynamic library of mixed ligand Zn_4L_6 cages, *Chem. Sci.*, 2016, **7**, 2614–2620.

7 (*a*) S. Leininger, B. Olenyuk and P. J. Stang, Self-assembly of discrete cyclic nanostructures mediated by transition metals, *Chem. Rev.*, 2000, **100**, 853–908; (*b*) M. Yoshizawa, J. K. Klosterman and M. Fujita, Functional molecular flasks: new properties and reactions within discrete, self-assembled hosts, *Angew. Chem., Int. Ed.*, 2009, **48**, 3418–3438; (*c*) R. Chakrabarty, P. S. Mukherjee and P. J. Stang, Supramolecular coordination: self-assembly of finite two- and three-dimensional ensembles, *Chem. Rev.*, 2011, **111**, 6810–6918; (*d*) T. R. Cook and P. J. Stang, Recent developments in the preparation and chemistry of metallacycles and metallacages via coordination, *Chem. Rev.*, 2015, **115**, 7001–7045; (*e*) A. J. McConnell, C. S. Wood, P. P. Neelakandan and J. R. Nitschke, Stimuli-responsive metal–ligand assemblies, *Chem. Rev.*, 2015, **115**, 7729–7793; (*f*) L.-J. Chen and H.-B. Yang, Construction of stimuli-responsive functional materials via hierarchical self-assembly involving coordination interactions, *Acc. Chem. Res.*, 2018, **51**, 2699–2710; (*g*) G.-Y. Wu, L.-J. Chen, L. Xu, X.-L. Zhao and H.-B. Yang, Construction of supramolecular hexagonal metallacycles via coordination-driven self-assembly: structure, properties and application, *Coord. Chem. Rev.*, 2018, **369**, 39–75; (*h*) H. Sepehrpour, W. Fu, Y. Sun and P. J. Stang, Biomedically relevant self-assembled metallacycles and metallacages, *J. Am. Chem. Soc.*, 2019, **141**, 14005–14020; (*i*) Y. Sun and P. J. Stang, Metallacycles, metallacages, and their aggregate/optical behavior, *Aggregate*, 2021, e94, DOI: 10.1002/agt2.94; (*j*) D. Zhang, T. K. Ronson, Y.-Q. Zou and J. R. Nitschke, Metal-organic cages for molecular separations, *Nat. Rev. Chem.*, 2021, **5**, 168–182.

8 (*a*) K. Acharyya, S. Bhattacharyya, H. Sepehrpour, S. Chakraborty, S. Lu, B. Shi, X. Li, P. S. Mukherjee and P. J. Stang, Self-assembled fluorescent Pt(II) metallacycles as artificial light-harvesting systems, *J. Am. Chem. Soc.*, 2019, **141**, 14565–14569; (*b*) T. Hong, Z. Zhang, Y. Sun, J.-J. Tao, J.-D. Tang, C. Xie, M. Wang, F. Chen, S.-S. Xie, S. Li and P. J. Stang, Chiral metallacycles as catalysts for asymmetric conjugate addition of styrylboronic acids to α,β-enones, *J. Am. Chem. Soc.*, 2020, **142**, 10244–10249; (*c*) Z. Zhang, Z. Zhao, L. Wu, S. Lu, S. Ling, G. Li, L. Xu, L. Ma, Y. Hou, X. Wang, X. Li, G. He, K. Wang, B. Zou and M. Zhang, Emissive platinum(II) cages with reverse fluorescence resonance energy transfer for multiple sensing, *J. Am. Chem. Soc.*, 2020, **142**, 2592–2600; (*d*) H. Zhu, Q. Li, B. Shi, H. Xing, Y. Sun, S. Lu, L. Shangguan, X. Li, F. Huang and P. J. Stang, Formation of planar chiral platinum triangles via pillar[5]arene for circularly polarized luminescence, *J. Am. Chem. Soc.*, 2020, **142**, 17340–17345; (*e*) P. Howlader, S. Mondal, S. Ahmed and P. S. Mukherjee, Guest-induced enantioselective self-assembly of a Pd_6 homochiral octahedral cage with a C_3-symmetric pyridyl donor, *J. Am. Chem. Soc.*, 2020, **142**, 20968–20972.

9 H.-W. Schmidt and F. Würthner, A periodic system of supramolecular elements, *Angew. Chem.*, 2020, **59**, 8766–8775.

10 (*a*) D. Whang, K.-M. Park, J. Heo, P. Ashton and K. Kim, Molecular necklace: quantitative self-assembly of a cyclic oligorotaxane from nine molecules, *J. Am. Chem. Soc.*, 1998, **120**, 4899–4900; (*b*) M. Fujita, N. Fujita, K. Ogura and K. Yamaguchi, Spontaneous assembly of ten components into two interlocked, identical coordination cages, *Nature*, 1999, **400**, 52–55; (*c*) K.-M. Park, S.-Y. Kim, J. Heo, D. Whang, S. Sakamoto, K. Yamaguchi and K. Kim, Designed self-assembly of molecular necklaces, *J. Am. Chem. Soc.*, 2001, **124**, 2140–2147; (*d*) Y. Liu, A. Bruneau, J. He and Z. Abliz, Palladium(II)-directed self-assembly of dynamic donor–acceptor [2]catenanes, *Org. Lett.*, 2008, **10**, 765–768; (*e*) C. Peinador, V. Blanco and J. M. Quintela, A

new doubly interlocked [2]catenane, *J. Am. Chem. Soc.*, 2009, **131**, 920–921; (*f*) R. S. Forgan, D. C. Friedman, C. L. Stern, C. J. Bruns and J. F. Stoddart, Directed self-assembly of a ring-in-ring complex, *Chem. Commun.*, 2010, **46**, 5861–5863; (*g*) V. Blanco, M. D. Garcia, C. Peinador and J. M. Quintela, Self-assembly of new fluorescent Pd(II) and Pt(II) 2,7-diazapyrenium-based metallocycles and study of their inclusion complexes and [3]catenane, *Chem. Sci.*, 2011, **2**, 2407–2411; (*h*) Z.-T. Zhang, Y.-M. Zhang and Y. Lu, Controlled molecular self-assembly behaviors between cucurbituril and bispyridinium derivatives, *J. Org. Chem.*, 2011, **76**, 4682–4685; (*i*) S. Freye, J. Hey, A. T. Galan, D. Stalke, R. H. Irmer, M. John and G. H. Clever, Allosteric binding of halide anions by a new dimeric interpenetrated coordination cage, *Angew. Chem., Int. Ed.*, 2012, **51**, 2191–2194; (*j*) S. P. Black, A. R. Stefankiewicz, M. M. J. Smulders, D. Sattler, C. A. Schalley, J. R. Nitschke and J. K. M. Sanders, Generation of a dynamic system of three-dimensional tetrahedral polycatenanes, *Angew. Chem., Int. Ed.*, 2013, **52**, 5749–5752; (*k*) H. Lee, P. Elumalai, N. Singh, H. Kim, S. U. Lee and K.-W. Chi, Selective synthesis of ruthenium(II) metalla[2]catenane via solvent and guest-dependent self-assembly, *J. Am. Chem. Soc.*, 2015, **137**, 4674–4677; (*l*) T. Sawada, M. Yamagami, K. Ohara, K. Yamaguchi and M. Fujita, Peptide [4]catenane by folding and assembly, *Angew. Chem., Int. Ed.*, 2016, **55**, 4519–4522; (*m*) G.-Y. Wu, X. Shi, H. Phan, H. Qu, Y.-X. Hu, G.-Q. Yin, X.-L. Zhao, X. Li, L. Xu, Q. Yu and H.-B. Yang, Efficient self-assembly of heterometallic triangular necklace with strong antibacterial activity, *Nat. Commun.*, 2020, **11**, 3178–3188; (*n*) J. Singh, D. H. Kim, E.-H. Kim, H. Kim, R. Hadiputra, J. Jung and K.-W. Chi, The first quantitative synthesis of a closed three-link chain (6_1^3) using coordination and noncovalent interactions-driven self-assembly, *J. Am. Chem. Soc.*, 2020, **142**, 9327–9336.

11 (*a*) S.-L. Huang, T. S. A. Hor and G.-X. Jin, Metallacyclic assembly of interlocked superstructures, *Coord. Chem. Rev.*, 2017, **333**, 1–26; (*b*) Y. Lu, H.-N. Zhang and G.-X. Jin, Molecular borromean rings based on half-sandwich organometallic rectangles, *Acc. Chem. Res.*, 2018, **51**, 2148–2158; (*c*) W.-X. Gao, H.-J. Feng, B.-B. Guo, Y. Lu and G.-X. Jin, Coordination-directed construction of molecular links, *Chem. Rev.*, 2020, **120**, 6288–6325; (*d*) L.-L. Dang, X. Gao, Y.-J. Lin and G.-X. Jin, Selective synthesis and structural transformation between a molecular ring-in-ring architecture and an abnormal trefoil knot, *Chem. Sci.*, 2020, **11**, 8013–8019; (*e*) Z. Cui, Y. Lu, X. Gao, H.-J. Feng and G.-X. Jin, Stereoselective synthesis of a topologically chiral solomon link, *J. Am. Chem. Soc.*, 2020, **142**, 13667–13671; (*f*) Y. Ye, Z.-P. Lin, W.-L. Jin, S.-P. Wang, J. Wu and S. Li, Self-assembly of mechanically interlocked structures via metal-mediated coordination cooperating with host-guest recognition, *Prog. Chem.*, 2015, **27**, 763–774; (*g*) T. Kim, N. Singh, J. Oh, E.-H. Kim, J. Jung, H. Kim and K.-W. Chi, Selective synthesis of molecular borromean rings: engineering of supramolecular topology via coordination-driven self-assembly, *J. Am. Chem. Soc.*, 2016, **138**, 8368–8371; (*h*) N. Singh, D. Kim, D. H. Kim, E.-H. Kim, H. Kim, M. S. Lah and K.-W. Chi, Selective synthesis of iridium(III)-derived molecular Borromean rings, [2]catenane and ring-in-ring macrocycles via coordination-driven self-assembly, *Dalton Trans.*, 2017, **46**, 571–577; (*i*) D. H. Kim, N. Singh, J. Oh, E.-H. Kim, J. Jung, H. Kim and K.-W. Chi, Coordination-driven self-assembly of a molecular knot comprising sixteen crossings, *Angew. Chem., Int. Ed.*, 2018, **57**, 5669–5673; (*j*) J. Singh, H. Kim and K.-W. Chi, Non-covalent interaction-directed coordination-driven self-assembly of non-trivial supramolecular topologies, *Chem. Rec.*, 2021, **21**, 574–593.

12 (*a*) S. Li, J. Huang, T. R. Cook, B. J. Pollock, H. Kim, K.-W. Chi and P. J. Stang, Formation of [3]catenanes from 10 precursors via multicomponent coordination-driven self-assembly of metallarectangles, *J. Am. Chem. Soc.*, 2013, **135**, 2084–2087; (*b*) S. Li, J. Huang, F. Zhou, T. R. Cook, X. Yan, Y. Ye, B. Zhu, B. Zheng and P. J. Stang, Self-assembly of triangular and hexagonal molecular necklaces, *J. Am. Chem. Soc.*, 2014, **136**, 5908–5911; (*c*) Y. Ye, S.-P. Wang, B. Zhu, T. R. Cook, J. Wu, S. Li and P. J. Stang, Self-assembly of [3]catenanes and a [4]molecular necklace based on a cryptand/paraquat recognition motif, *Org. Lett.*, 2015, **17**, 2804–2807.

13 (*a*) V. Blanco, M. Chas, D. Abella, E. Pía, C. Platas-Iglesias, C. Peinador and J. M. Quintela, Self-assembly of 1: 2 inclusion complexes between a metallocycle host and dihydroxyaromatic guests: a redox controlled complexation process, *Org. Lett.*, 2008, **10**, 409–412; (*b*) V. Blanco, M. Chas, D. Abella, C. Peinador and J. M. Quintela, Molecular catenation via metal-directed self-assembly and π-donor/π-acceptor interactions: efficient one-pot synthesis, characterization, and crystal structures of [3]catenanes based on Pd or Pt dinuclear metallocycles, *J. Am. Chem. Soc.*, 2007, **129**, 13978–13986.

14 P. Job, Formation and Stability of Inorganic Complexes in Solution, *Ann. Chim.*, 1928, **9**, 113–203.

